



# HHS Public Access

## Author manuscript

*J Anal At Spectrom.* Author manuscript; available in PMC 2022 June 06.

Published in final edited form as:

*J Anal At Spectrom.* 2018 ; 33(3): 404–412. doi:10.1039/c7ja00252a.

## Calibration Approaches for Measurement of Aerosol Multielemental Concentration using Spark Emission Spectroscopy

L. Zheng<sup>a,b</sup>, P. Kulkarni<sup>a,†</sup>, D. D. Dionysiou<sup>b</sup>

<sup>a</sup>Centers for Disease Control and Prevention, National Institute for Occupational Safety and Health, Cincinnati, OH 45226, USA.

<sup>b</sup>Environmental Engineering and Science Program, Department of Biomedical, Chemical, and Environmental Engineering, University of Cincinnati, OH, 45221, USA.

### Abstract

A multivariate calibration approach, using partial least squares regression, has been developed for measurement of aerosol elemental concentration. A training set consisting of 25 orthogonal aerosol samples with 9 factors (elements: Cr, Mn, Fe, Ni, Cu, Zn, Cd, Pb, Ti) and 5 levels (elemental concentrations) was designed. Spectral information was obtained for each aerosol sample using aerosol spark emission spectroscopy (ASES) at a time resolution of 1 minute. Simultaneous filter samples were collected for determination of elemental concentration using an inductively coupled plasma mass spectrometry (ICP-MS) analysis. Two regression models, PLS1 and PLS2, were developed to predict mass concentration from spectral measurements. Prediction ability of the models improved substantially when only signature wavelengths were included instead of the entire spectrum. The PLS1 model with 45 selected spectral variables (PLS1-45 model) presented the lowest relative root mean square error of cross validation (RMSECV; 16 - 35%). The detection limits using the PLS1-45 model, for the nine elements were in the range of 0.16 – 0.50  $\mu\text{g}/\text{m}^3$ . The performance of both multivariate and univariate regression models were tested for an unknown sample of welding fume aerosol. The multivariate model did not provide significantly better prediction compared to the univariate model. In spite of the difference in matrices of calibration aerosol and the unknown test aerosol, the results from PLS model show good agreement with those from filter measurements. The relative root mean square error of prediction (RMSEP) obtained from PLS1-45 model was 13% for Cr, 23% for Fe, 22% for Mn and 12% for Ni. The study shows that in spite of lower spectral resolution and lack of sample preparation, reliable and robust measurements can be obtained using the proposed calibration method based on PLS regression.

---

<sup>†</sup>Author to whom correspondence should be addressed to: Phone: (513) 841-4300; Fax: (513) 841-4545; PSKulkarni@cdc.gov.

Electronic Supplementary Information (ESI) available: [Univariate calibration curves and PLS regression coefficient plots]. See DOI: [10.1039/x0xx00000x](https://doi.org/10.1039/x0xx00000x)

## 1 Introduction

Exposure to airborne particles containing toxic metals in industrial atmospheres have adverse health effects on workers, thereby prompting the need for reliable measurement methods for exposure characterization. The most widely used methods for determining concentrations of particulate toxic metals involve filter collection over several hours, followed by off-line analyses.<sup>1, 2</sup> These methods are time-consuming and cannot capture short-term exposures. Workers cannot obtain instant feedback on their exposure to inhalable hazards. Developing real-time methods for measuring aerosol chemical composition is of great significance to instantaneously assess exposure risks.

Our group has investigated various field portable microplasma spectroscopy techniques for real-time measurement of elemental species in aerosol particles<sup>3-6</sup> using broadband liquid crystal display (LCD) spectrometers. These techniques include laser-induced breakdown spectroscopy (LIBS), spark emission spectroscopy (SES) and glow discharge optical emission spectroscopy (GD-OES), and allow simultaneous multielemental measurement of aerosol. While these methods offer several practical advantages with respect to development of low-cost, hand-portable instruments for exposure monitoring, they also suffer from drawbacks relating to relatively inferior analytical figures of merit (compared to laboratory instruments) owing to lack of optimal sample preparation and reduced wavelength resolution of LCD spectrometers. The objective of this study was to investigate the usefulness of multivariate calibration approaches to improve calibration of microplasma methods for multielemental aerosol analysis.

For quantitative analysis of aerosols using microplasma spectroscopy, a univariate calibration approach has been widely used to construct calibration curves for relating the signal intensity and elemental concentration or mass.<sup>3, 4, 7-10</sup> However, in most spectroscopic methods, quantitative spectral analyses remains challenging due to sample matrix effects (physical and chemical matrix effects) and spectral interferences.<sup>11</sup> The emission signal intensity from one element is affected, among other factors, by the overall chemical composition of the sample. These matrix effects can result in large uncertainties if univariate calibration methods are used, especially when unknown samples have different chemical matrices from the calibration standards.<sup>12-14</sup> To minimize the sample matrix effects, matrix-matched standards are often used for univariate calibration in spectroscopic methods.<sup>15, 16</sup> However, preparation and certification of matrix-matched standards are tedious for a given analytical measurement.

The application of multivariate calibration in spectroscopic analysis has proved to be beneficial in accounting for matrix effects as well as eliminating spectral interferences.<sup>13, 17</sup> Multivariate calibration has been widely used for analysis of natural samples (such as rubber antioxidants, diesel fuel, seeds, and wine fermentations) by near-infrared (NIR) spectroscopy which usually presents relatively weak and highly overlapping spectral bands.<sup>18-22</sup> Multivariate calibration has also been employed in atomic emission spectroscopy for elemental analysis of mixtures, such as steels, alloys, coal, and soil.<sup>23-27</sup> Unburned carbon in fly ash was analysed using LIBS and showed that the multivariate calibration had better performance than univariate calibration as matrix effects caused by other components in fly

ash could be taken into account.<sup>13</sup> Comparison of single and multivariate calibration for determination of Si, Mn, Cr and Ni in high-alloyed stainless steels using LIBS has shown that multivariate analysis of spectral data was more effective and accurate when analytical lines overlapped.<sup>17</sup>

In this paper, we present a multivariate calibration approach for simultaneous measurement of multiple elements in aerosols using SES. Partial least squares (PLS) regression was used with a calibration training set to build PLS models for predicting elemental concentration of aerosols. The prediction capability of the PLS models (PLS1 and PLS2) with different configurations were compared for unknown test sample of welding fume aerosol.

## 2 Methods

### 2.1 Instrumentation

Spark emission spectroscopy was used for quantitative measurement of elemental concentration of aerosols. The details of this method are described elsewhere.<sup>4, 5, 28</sup> Briefly, this method involves collection of particles onto a small electrode tip (500  $\mu\text{m}$  in diameter) with a corona aerosol microconcentrator (CAM)<sup>28</sup>, followed by ablation of particles by a spark produced using a high voltage (HV) pulse generator (200 mJ per pulse; ARC-2, Cascodium Inc., Andover, MA). The optical emission from excited atomic and ionic species in the spark-induced plasma was collected by a broadband spectrometer (200 – 900 nm wavelength range, 0.1 nm resolution; LIBS 2500 Plus; Ocean Optics Inc.; Dunedin, FL) for spectrochemical analysis. A delay time of 5  $\mu\text{s}$  and a gate width of 1 ms were used. The spectral data were used to identify elements and determine their mass in the collected particle samples.

### 2.2 Calibration Aerosols

Aerosol containing metals of interest were generated from solutions using a pneumatic atomizer (model 3076, TSI Inc., Shoreview, MN). The precursor solutions used in the atomizer were prepared using water-soluble nitrates of analytes of interest. A multilevel multifactor training set, containing various metals at various concentration levels, was designed for multivariate calibration.<sup>29</sup> It consisted of 25 samples with 9 mutually orthogonal factors (i.e., elements: Cr, Mn, Fe, Ni, Cu, Zn, Cd, Pb, Ti) and 5 levels (elemental concentration in solution), as shown in Table 1.

### 2.3 Experimental procedure

Fig. 1 shows the schematic diagram of the multivariate calibration experimental procedure for measurement of aerosol elemental concentrations. Test aerosol was generated using a pneumatic atomizer, then passed through a diffusion dryer. The dry aerosol was introduced into a CAM for near real-time analysis using SES. The particles were collected in CAM for 1 minute at a flow rate of 2 L  $\text{min}^{-1}$ , followed by SES measurement following procedures described elsewhere.<sup>4, 5</sup> Test aerosol sample was analysed by SES in five consecutive measurements (the relative standard deviation of signal intensity was less than 15%), and their average was used to obtain the spectra for each sample. The same test aerosol was also simultaneously collected on a polyvinyl chloride (PVC) filter for subsequent off-line

elemental analysis. The particles were collected for 30 minutes at a flow rate of 2 L min<sup>-1</sup>. Each filter sample was digested following NIOSH Method 7303 (Hot Block/HCl/HNO<sub>3</sub> Digestion) and then analysed using inductively coupled plasma mass spectrometry (ICP-MS). ICP-MS was used for filter sample analysis in this study because of its superior detection limits compared to ICP-AES for most elements. Very low detection limits were desirable in this study due to short collection times (for filter samples) used in this study. Studies have shown that ICP-MS has far superior recoveries (~100%) and precision (<0.2) for determination of metals in filter samples.<sup>30</sup> The elemental masses of the aerosol particles collected on the electrode in CAM were deduced from the elemental air concentrations obtained from filter collection and ICP-MS analysis, and are shown in Table 2. A model was constructed using PLS regression as described below.

#### 2.4 PLS regression model

A PLS model was constructed by using the measured spectra for all the test aerosols generated from the 'training set' calibration solutions. The model involves a linear regression between predictor/explanatory variables  $\lambda_i$  and response/dependent variables  $m_j$ . For each measurement, the predicted mass for element  $j$ ,  $m_j$  is given by,

$$m_j = \sum_{i=0}^p \beta_{ji} \lambda_i + \epsilon_j \quad (1)$$

where,  $\lambda_i$  is the signal intensity at wavelength  $i$  of emission spectra,  $\beta_{ji}$  the linear regression coefficient for element  $j$  at each wavelength of emission spectra and  $\epsilon_j$  is a noise term for element  $j$ .  $p$  is the number of selected discrete wavelengths in each emission spectra.

The general matrix equation for the entire data takes the following form:

$$\begin{aligned} \lambda_{np} &= \mathbf{TP}^T + \mathbf{\epsilon}_1 \\ \mathbf{m}_{nq} &= \mathbf{UQ}^T + \mathbf{\epsilon}_2 \end{aligned} \quad (2)$$

where  $\lambda_{np}$  is an  $n \times p$  matrix of predictor variables,  $\mathbf{m}_{nq}$  is an  $n \times q$  matrix of response variables;  $\mathbf{T}$  and  $\mathbf{U}$  matrices represent the projections of  $\lambda_{np}$  and  $\mathbf{m}_{nq}$ , respectively;  $\mathbf{P}$  and  $\mathbf{Q}$  represent the matrices of loadings of the original variables; and  $\mathbf{\epsilon}_1$  and  $\mathbf{\epsilon}_2$  are the residual matrices related to the noise. In this study,  $n = 25$ , corresponds to the number of total samples in the training set. The number of explanatory variables  $p$  is same as the number of wavelengths included in the emission spectra. Also the number of response variables  $q$  is same as the number of elements in each sample in the training set, and  $q = 9$ .

Two types of models were constructed for each analyte: model PLS1 and model PLS2. In model PLS1, only one element was modelled each time (i.e. nine separate PLS1 models were built for each element), while all nine elements were simultaneously used in a single PLS2 model.<sup>31</sup> Different number of explanatory variables (i.e. signal intensity) were selected as model inputs to build various models. The number of latent variables for each model was chosen to correspond to the lowest root mean square error of the cross validation (RMSECV),<sup>32</sup> which typically ranged from 3–6 ng. Cross validation, which involves verifying the prediction capability of the PLS model, was performed using the 'leave-one-

out' method. In this method, only one sample at a time is left out of the calibration and the remaining samples are used for constructing a model to predict the sample that has been left out.<sup>32</sup> This procedure is repeated until all samples have been left out once. The performance of the regression models were evaluated by examining their relative RMSECV and correlation coefficients  $R^2$  of cross validation. The PLS analyses were carried out using the software The Unscrambler 10.0 X (CAMO Software Inc., Woodbridge, NJ).

### 3 Results and discussion

#### 3.1 Wavelength selection

Several studies involving chemometric analysis of spectroscopic data have employed select wavelengths as the explanatory variables, and have shown that the prediction ability of multivariate regression models could be improved when using the wavelengths that capture or explain maximum variance in the analyte concentration.<sup>33, 34</sup> In this study, PLS regression coefficients were used for selection of the most relevant wavelengths for each Y response variable (i.e., elemental mass).<sup>33-35</sup> The wavelengths which have larger regression coefficients represent the emission signals that are better correlated to the mass of analyte.

Fig. 2 shows the PLS1 regression coefficients for Cr in the wavelength range of 300 – 540 nm. Highest regression coefficients were observed around 520 nm wavelength. The magnified inset (Fig. 2(c)) presents three overlapping peaks around 520 nm. These three peaks are consistent with the Cr atomic emission lines: Cr I 520.45 nm, Cr I 520.60 nm, and Cr I 520.84 nm, according to the National Institute of Standards and Technology (NIST) atomic spectral database. In addition to the triplet peak, there are three consecutive peaks observed around 360 nm (Fig. 2(a)), 425 nm (Fig. 2(b)) and 530 nm (Fig. 2(d)), respectively. They correspond to Cr I emission lines at 357.87 nm, 359.35 nm, 360.53 nm, 425.43 nm, 427.48 nm, 428.97 nm, 529.82 nm, 532.83 nm and 534.58 nm according to the NIST atomic spectral database. Similar relevant wavelengths for all the other elements of interest in this study were chosen by analysing their PLS regression coefficients. The PLS1 regression coefficients for all the remaining elements are shown in Fig. S1 in the Supplemental Information. Five explanatory variables for each emission peak (central wavelength pixel, including two additional pixels on each side) were used. For each element, wavelengths with regression coefficients greater than three times the standard deviation ( $3\sigma$ ) around the mean regression coefficient (over all the wavelengths) were selected for subsequent verification. Table 3 shows the emission lines we have verified for each element based on NIST atomic spectra database (ASD). These lines are not identified as self-absorbing or self-reversing lines in the ASD. The emission lines highlighted in bold were chosen to construct PLS1-45 and univariate regression models for each element; these lines exhibit relatively higher regression coefficients and minimal spectral interference.

#### 3.2 Multivariate calibration using PLS

Both PLS1 and PLS2 models were built by constructing the relationship between elemental mass and spectra. For constructing the PLS1 model, only one analyte was chosen as the response variable  $\mathbf{m}_{nj}$  ( $j = 1, 2, \dots, \text{or } 9$ ). Here, nine PLS1 models were constructed separately for each analyte (i.e. response variable). For the PLS2 model, all the nine

response variables  $m_{nq}$  were chosen as the response variables simultaneously. Three  $\lambda_{np}$  matrices with different number of variables were selected as explanatory variables to build various PLS models. These three  $\lambda_{np}$  matrices include: (i) explanatory variables containing the whole spectra ranging from 300 to 540 nm (4312 variables), (ii) significant explanatory variables containing multiple emission peaks related to the analytes (all the emission peaks shown in Table 3, i.e., 290 variables), and (iii) a subset of significant explanatory variables containing only one emission peak for each element (i.e., the ones with relatively higher regression coefficient and minimal spectral interference with other elements, highlighted in Table 3; 45 variables in total for all the nine elements). To simplify the model description, these models were denoted as PLS1-4312, PLS1-290, PLS1-45, PLS2-4312, PLS2-290, and PLS2-45, respectively.

Table 4 shows the relative RMSECV and  $R^2$  obtained from cross validation for different models. Comparison of the PLS models constructed with different numbers of variables shows that the models with selected variables (PLS1-290, PLS1-45, PLS2-290, and PLS2-45) were significantly superior to the models with the whole spectra (PLS1-4312 and PLS2-4312). For PLS1 models, as the variable number is reduced from 4312 to 45, the average relative RMSECV for the nine elements is reduced from 36% to 25% and the average  $R^2$  is improved from 0.65 to 0.84. This result demonstrates that variable selection plays an important role in multivariate calibration for elemental mass using spark emission spectroscopy. Although the PLS model has the ability to deal with numerous variables, the error of prediction could deteriorate if the entire raw spectral data are used in the calibration, because the majority of data consist of noise. Therefore, the use of selected explanatory variables that are most relevant to the underlying phenomenon as input variables is essential to construct the optimal PLS model. Comparison of PLS1 models using the selected wavelengths (PLS1-290 and PLS1-45) shows that their prediction abilities are quite similar. This is because the signal intensities of multiple emission peaks from the same element are correlated. Selection of one emission peak for each element as input variables of the PLS model is sufficient for constructing accurate multivariate models. Of all the nine elements, Fe and Pb show low  $R^2$  values, likely due to the high detection limits of Fe and Pb in our system (the detection limits are shown in Table 5). In this study, the elemental concentration of Fe and Pb in the calibration aerosol were close to their limit of quantification, leading to increased measurement uncertainty and poor  $R^2$ .

Table 4 also shows that the relative RMSECVs of PLS1 models are 2 – 4% smaller than PLS2 models. This suggests that the PLS1 models have lower error than the PLS2 models. However, the need to construct a separate model for each element is a drawback of PLS1 approach. On the other hand, one PLS2 model can be applied simultaneously to all the elements and is easier to implement.

Using the 25 multielement samples in the training set, a univariate regression model (U-ME) was also constructed for each element by plotting the signal intensity of an emission line as a function of elemental mass. For each element, the emission line with the highest regression coefficient was used. The signal intensity of an emission line was calculated as either the peak height or the peak area, both after baseline correction. The U-ME models were described using linear regression curves. These univariate calibration curves

(based on peak height) are shown in Fig. S2 in the Supplemental Information. The  $R^2$  and RMSE of the univariate regression are also shown in Table 4. The  $R^2$  values in the parenthesis are obtained from univariate regression using peak area for each element. Both the peak height- and peak area-based calibration curves yielded similar sensitivity. For most elements, the U-ME model gives similar  $R^2$  and RMSE values to those of the PLS models with select variables (i.e. PLS1-290, PLS1-45, PLS2-290, and PLS2-45). There is no consistent evidence in the literature about the effectiveness of different calibration methods (i.e. multivariate and univariate methods).<sup>13, 14, 17</sup> For example, some studies on sample analysis using LIBS suggest that multivariate calibration provides improved accuracy and precision compared with univariate calibration,<sup>13, 14</sup> while another study on determination of elements in stainless steels using LIBS showed that the univariate calibration provided the best prediction if appropriate, non-overlapping emission lines could be found.<sup>17</sup> To a certain extent, the performance of different calibration approaches depends on both spectral overlap and design of the calibration experiments.<sup>36</sup> In this study, we designed the training set with orthogonal factors (using elements relevant to welding aerosol measurement) and selected the non-overlapping emission peaks for calibration. Both the univariate and multivariate calibration approaches showed similar prediction capability.

Fig. 3 shows comparison of calibration values (open circle) with the corresponding cross-validation (solid triangle) for the PLS1-45 model. The mass predicted by the model is plotted on the y-axis and corresponding to the measured mass on the x-axis. These models were constructed with 9, 5, 6, 5, 3, 4, 3, 6, 5 latent variables for Cr, Mn, Fe, Ni, Cu, Zn, Cd, Pb, and Ti, respectively. The PLS regression results (open circle) show a strong correlation between the predicted and measured elemental mass, with  $R^2$  values in the range of 0.81 – 0.96 for different elements. The cross validation results (solid triangle) also show a strong correlation with an average  $R^2$  values of 0.84. The relative RMSECV of PLS1-45 models for different elements is in the range of 16 – 35%. For Fe low  $R^2$  (0.71) and high RMSECV (35%) were observed, probably due to the poor detection limits of Fe in our system (the detection limit is shown in Table 5). A large uncertainty might be produced when the elemental mass concentration of calibration aerosol is near the limits of quantification. Matrix effects may also have been relatively more significant for Fe measurement.

### 3.3 Limits of detection

According to 3- $\sigma$  criteria defined by the International Union of Pure and Applied Chemistry (IUPAC),<sup>37</sup> the limit of detection (LOD) for univariate calibration is expressed as,

$$m_{LOD} = \frac{3\sigma}{S} \quad (3)$$

where  $\sigma$  is the standard deviation of the blank at the selected emission line and  $S$  the sensitivity given by the slope of the calibration curve of univariate calibration. Blank measurements were taken and  $\sigma$  was obtained by averaging over 20 replicate blank measurements.

LOD in multivariate calibration was determined analogously to the univariate calibration:<sup>38, 39</sup>

$$m_{LOD} = \frac{3.3\sigma}{S} = 3.3\sigma\|b\| = 3.3\sigma\sqrt{b_1^2 + \dots + b_n^2} \quad (4)$$

where  $\sigma$  is an estimate of the noise level in the data,  $S$  is the sensitivity of the PLS model, that gives the fraction of analytical signal due to the increase of the concentration of a particular analyte at unit concentration,  $\|b\|$  is the Euclidian norm of the regression coefficients vector, and  $b_n$  is the  $n^{th}$  regression coefficient.  $\sigma$  was obtained by measuring the variation of the noise in the selected regions for each analyte.  $S$  was estimated as the inverse of  $\|b\|$ . Table 5 shows the LOD obtained from both univariate calibration and multivariate calibration (PLS1-45 model) for elemental measurement using SES. The mass LOD for multivariate calibration is in the range of 0.8 – 2.5 ng depending on the element, with the lowest LOD for Cd and the highest LOD for Fe. The LOD for multivariate calibration is in the range of 0.16 – 0.50  $\mu\text{g m}^{-3}$  in terms of air concentration, calculated by assuming a flow rate of 2  $\text{L min}^{-1}$ , a collection time of 5 minutes, and particle collection efficiency of 0.5 for our system. Comparison of the LODs from univariate and multivariate calibration shows that both approaches provide similar LODs for most elements (except Fe, Ni, and Pb). This result is consistent with that found by Braga et al. in their study on comparison of univariate and multivariate calibration for determination of micronutrients in plant materials using LIBS.<sup>37</sup> It is worth noting that the LOD for Fe, Ni, and Pb from univariate calibration is nearly twice that from the multivariate calibration. This difference could possibly be due to higher measurement uncertainties for these elements arising from matrix effects.

### 3.4 Application to welding aerosol measurement

We applied the multivariate regression models (PLS1-45 and PLS1-290), developed using the training set, to the measurement of unknown elemental concentration of welding aerosol. Test welding aerosol was generated by aerosolizing suspension of stainless steel welding fume reference material (HSL SSWF-01, Health & Safety Laboratory, Buxton, UK). It should be noted that the matrix composition of this reference material (i.e., number of elements and their relative concentration in the matrix) and their solubility are different from that of the calibration samples (Table 1). The compounds used for calibration were soluble, while the welding fume particles were insoluble. From the suspension containing welding fume reference material, aerosols with five different air concentration levels were obtained through dilution of the aerosol with clean, particle-free air. Test aerosols were collected for 2 minutes using the ASES system at 2  $\text{L min}^{-1}$ . The elemental masses in the collected samples were predicted using both multivariate and univariate regression models, and then inverted to elemental air concentrations. Three repeat measurements were performed by ASES for each test aerosol sample. Simultaneously, filter samples were collected (for 30 min) in parallel to obtain the elemental concentrations of test welding aerosol by laboratory ICP-MS analysis after sample digestion. The test aerosols were relatively stable during these 30 minutes.

Fig. 4 shows the comparison of elemental concentration predicted by the regression models: (a) PLS1-45 model, (b) PLS1-290 model, (c) univariate calibration from single element solutions (U-SE model). Model predictions are compared with corresponding ICP-MS measurements shown on x-axis. Fig. 4 shows that most (17 out of 20 for PLS1-45 model, 16 out of 20 for PLS1-290 model, and 15 out of 20 for U-SE model) samples agreed with the

ICP-MS measurements within the  $\pm 25\%$  bias. The results from the multivariate models [Fig. 4 (a) and (b)] show good agreement with those from filter samples using ICP-MS. However, it is worth noting that the univariate calibration curve exhibits non-linear behaviour at higher mass loadings. The effect was not pronounced at mass loadings studied in this work; however, the extrapolation of the curve seems to suggest significantly nonlinear behaviour at mass loadings above  $100 \mu\text{g}/\text{m}^3$  [Fig. 4 (c)]. In spite of the difference in matrices, with respect to solubility and elemental composition, of calibration aerosol and welding fume aerosol, the agreement between ASES measurements and the ICP-MS measurements is good. This demonstrates that the prediction models constructed using particles aerosolized from soluble precursor species could be reliably used for measurement of unknown insoluble (or soluble) particles using ASES. This significantly simplifies calibration of field portable ASES instruments.

Relative root mean square error of prediction (RMSEP) was used to estimate the accuracy of our regression models. The relative RMSEP from the PLS1-45 model was 13% for Cr, 23% for Fe, 22% for Mn and 12% for Ni. The relative RMSEP from the PLS1-290 model was 12% for Cr, 25% for Fe, 21% for Mn and 13% for Ni. The relative RMSEP from the U-SE model was 14% for Cr, 27% for Fe, 29% for Mn and 10% for Ni. Multivariate calibration approach resulted in slightly better prediction accuracy than the single element univariate calibration approach when they were applied to measurement of welding fume aerosol. The welding aerosol represented a smaller subset of calibration aerosol in terms of the number of elements—the calibration aerosol had nine elements; whereas the welding aerosol had only four elements. Moreover, as noted above, unlike the calibration aerosols, the welding aerosol particles were insoluble in water. The matrix effects in these samples may not be pronounced, which may explain somewhat similar results from both univariate and multivariate methods. However, the multivariate method may provide better precision in cases where significant matrix effects or nonlinear calibration curve are expected. Multivariate methods should also provide better precision and accuracy for cases involving significant spectral overlap or interference for analytes of interest.

The error bars in Fig. 4 show the standard deviation of three replicate measurements, which ranged from 7 – 19%, demonstrating good precision of the ASES aerosol measurement system.

## Conclusions

A multivariate calibration approach for measurement of aerosol elemental concentrations by SES was developed. The orthogonal training set design (Table 1) in combination with suitable multivariate calibration allows one to make full use of the multielemental emission spectra without the loss of spectral selectivity. It was shown that PLS regression coefficients can be judiciously used as a guide for selecting most relevant portions of the emission spectra and allow construction of meaningful multivariate regression models.

Separate PLS models for single element (i.e. model PLS1) offers slightly improved prediction ability than a single PLS model for multiple elements (model PLS2). Using a training set with orthogonal factors, it was found that multivariate models provided slightly

better prediction compared to the univariate model. The simplicity of univariate calibration methods may be more attractive in applications where the unknown matrix has fewer elements and is relatively homogenous. However, multivariate calibration may be preferable for aerosol particles containing large numbers of elements with highly varying elemental ratios. The multivariate model may also provide better precision when significant spectral interferences or overlapping is expected.

Application of the PLS models to welding aerosol also showed good agreement with ICP-MS measurements in spite of significant difference in calibration sample matrix (9 elements; soluble compounds) and unknown sample (4 elements; insoluble compounds). In spite of relatively lower spectral resolution and lack of sample preparation in our ASES method, good agreement with the ICP-MS method suggests that using PLS regression with an orthogonal training set provides a relatively robust calibration method for field-portable microplasma methods for elemental analysis.

## Supplementary Material

Refer to Web version on PubMed Central for supplementary material.

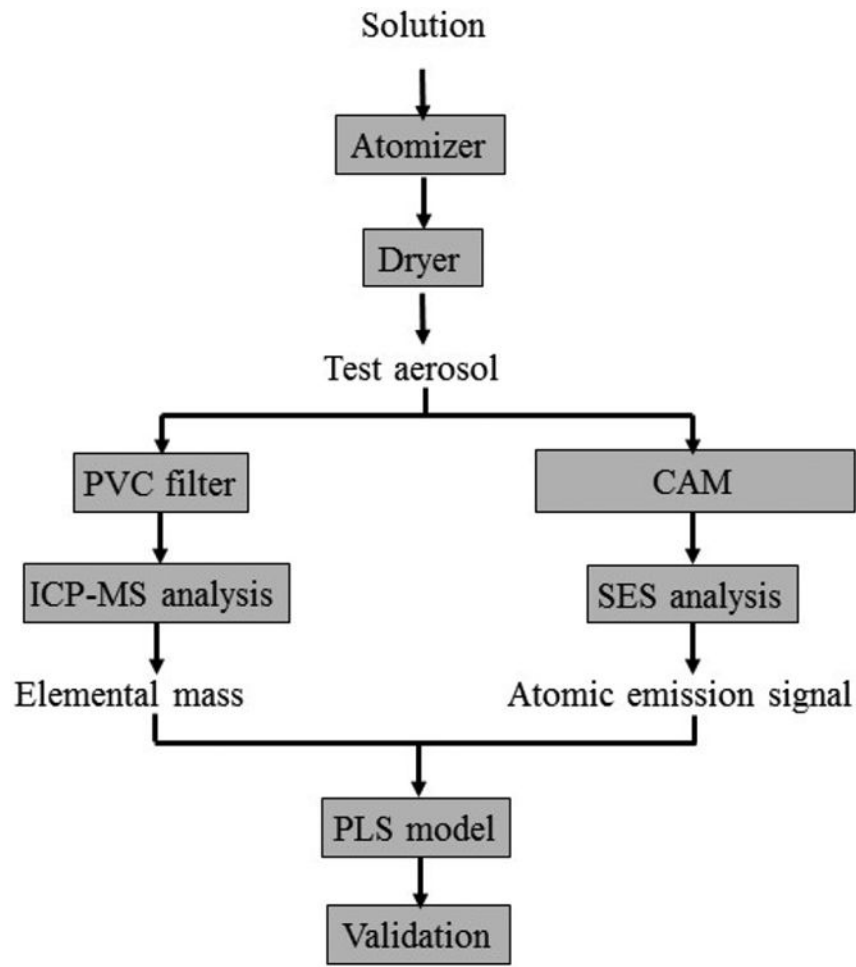
## Acknowledgements

This research work is supported by intramural NORA and NTRC grants at NIOSH (CAN ZKPY, ZJLS, and ZLFX). Authors would like to thank Dr. Kevin Ashley and Amy Feng for providing helpful feedback and review of this manuscript.

## References

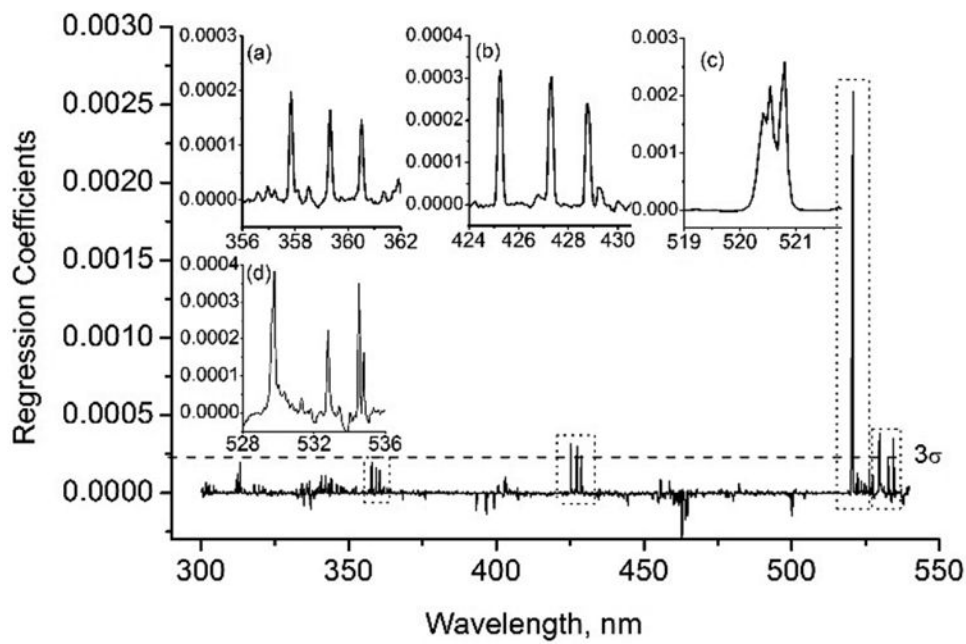
1. Raynor PC, Leith D, Lee K and Mukund R, in *Aerosol Measurement: Principles, Techniques and Applications*, eds. Kulkarni P, Baron PA and Willeke K, John Wiley & Sons, Hoboken, New Jersey, 2011, ch. 7.
2. Spurny KR, *Analytical Chemistry of Aerosols: Science and Technology*, CRC Press, Boca Raton, Florida, 1999.
3. Diwakar P, Kulkarni P and Birch ME, *Aerosol Sci. Technol.*, 2012, 46, 316–332. [PubMed: 26692632]
4. Diwakar PK and Kulkarni P, *J. Anal. At. Spectrom.*, 2012, 27, 1101–1109. [PubMed: 26491209]
5. Zheng L, Kulkarni P, Birch ME, Deye G and Dionysiou DD, *Aerosol Sci. Technol.*, 2016, 50, 1155–1166. [PubMed: 28638174]
6. Zheng L and Kulkarni P, *Anal. Chem.*, 2017, 89, 6551–6558. [PubMed: 28513144]
7. Martin MZ, Cheng MD and Martin RC, *Aerosol Sci. Technol.*, 1999, 31, 409–421.
8. Hunter AJR, Davis SJ, Piper LG, Holtzclaw KW and Fraser ME, *Appl. Spectrosc.*, 2000, 54, 575–582.
9. Khalaji M, Roshanzadeh B, Mansoori A, Taefi N and Tavassoli SH, *Opt. Laser Eng.*, 2012, 50, 110–113.
10. Marcus RK, Dempster MA, Gibeau TE and Reynolds EM, *Anal. Chem.*, 1999, 71, 3061–3069. [PubMed: 21662898]
11. Gemperline P, *Practical Guide to Chemometrics*, CRC press, Boca Raton, Florida, 2006.
12. Laville S, Sabsabi M and Doucet FR, *Spectrochim. Acta, Part B*, 2007, 62, 1557–1566.
13. Yao S, Lu J, Zheng J and Dong M, *J. Anal. At. Spectrom.*, 2012, 27, 473–478.
14. Tripathi MM, Eseller KE, Yueh F-Y and Singh JP, *Spectrochim. Acta, Part B*, 2009, 64, 1212–1218.

15. Cremers DA and Radziemski LJ, *Handbook of Laser-Induced Breakdown Spectroscopy*, John Wiley & Sons, Chichester, England, 2006, pp99–117.
16. da Silva Gomes M, de Carvalho GGA, Santos D and Krug FJ, *Spectrochim. Acta, Part B*, 2013, 86, 137–141.
17. Zaytsev SM, Popov AM, Chernykh EV, Voronina RD, Zorov NB and Labutin TA, *J. Anal. At. Spectrom.*, 2014, 29, 1417–1424.
18. Boschetti CE and Olivieri AC, *J. Near Infrared Spec.*, 2001, 9, 245–254.
19. Breitkreitz MC, Raimundo IM, Rohwedder JJR, Pasquini C, Dantas HA, Jose GE and Araujo MCU, *Analyst*, 2003, 128, 1204–1207. [PubMed: 14529031]
20. Lestander TA and Geladi P, *Can. J. Forest Res.*, 2005, 35, 1139–1148.
21. Shao X, Bian X, Liu J, Zhang M and Cai W, *Anal. Methods*, 2010, 2, 1662–1666.
22. Zeaiter M, Roger JM and Bellon-Maurel V, *Chemometr. Intell. Lab.*, 2006, 80, 227–235.
23. Martin MZ, Labb   N, Andr   N, Wullschleger SD, Harris RD and Ebinger MH, *Soil Sci. Soc. Am. J.*, 2010, 74, 87–93.
24. Doucet FR, Belliveau TF, Fortier J-L and Hubert J, *Appl. Spectrosc.*, 2007, 61, 327–332. [PubMed: 17389074]
25. Golloc A and Wilke K, *J. Anal. At. Spectrom.*, 1997, 12, 1225–1230.
26. Gonzaga FB and Pasquini C, *Spectrochim. Acta, Part B*, 2012, 69, 20–24.
27. Feng J, Wang Z, Li L, Li Z and Ni W, *Appl. Spectrosc.*, 2013, 67, 291–300. [PubMed: 23452493]
28. Zheng L, Kulkarni P, Zavvos K, Liang H, Birch ME and Dionysiou DD, *J. Aerosol Sci.*, 2017, 104, 66–78. [PubMed: 28626243]
29. Brereton RG, *Analyst*, 1997, 122, 1521–1529.
30. Ashley K, Shulman SA, Brisson MJ and Howe AM, *J. Environ. Monitor.*, 2012, 14, 360–367.
31. Brereton RG, *Analyst*, 2000, 125, 2125–2154.
32. Brereton RG, *Applied Chemometrics for Scientists*, John Wiley & Sons, Chichester, England, 2007.
33. Frenich AG, Jouan-Rimbaud D, Massart DL, Kuttatharmmakul S, Galera MM and Vidal JLM, *Analyst*, 1995, 120, 2787–2792.
34. Xu H, Liu Z, Cai W and Shao X, *Chemometr. Intell. Lab.*, 2009, 97, 189–193.
35. Osborne SD, K  nnemeyer R and Jordan RB, *Analyst*, 1997, 122, 1531–1537.
36. Demir C and Brereton RG, *Analyst*, 1998, 123, 181–189.
37. Boumans P, *Anal. Chem.*, 1994, 66, 459A–467A.
38. Valderrama P, Braga JWB and Poppi RJ, *J. Agric. Food Chem.*, 2007, 55, 8331–8338. [PubMed: 17927144]
39. Braga JWB, Trevizan LC, Nunes LC, Rufini IA, Santos D and Krug FJ, *Spectrochim. Acta, Part B*, 2010, 65, 66–74.

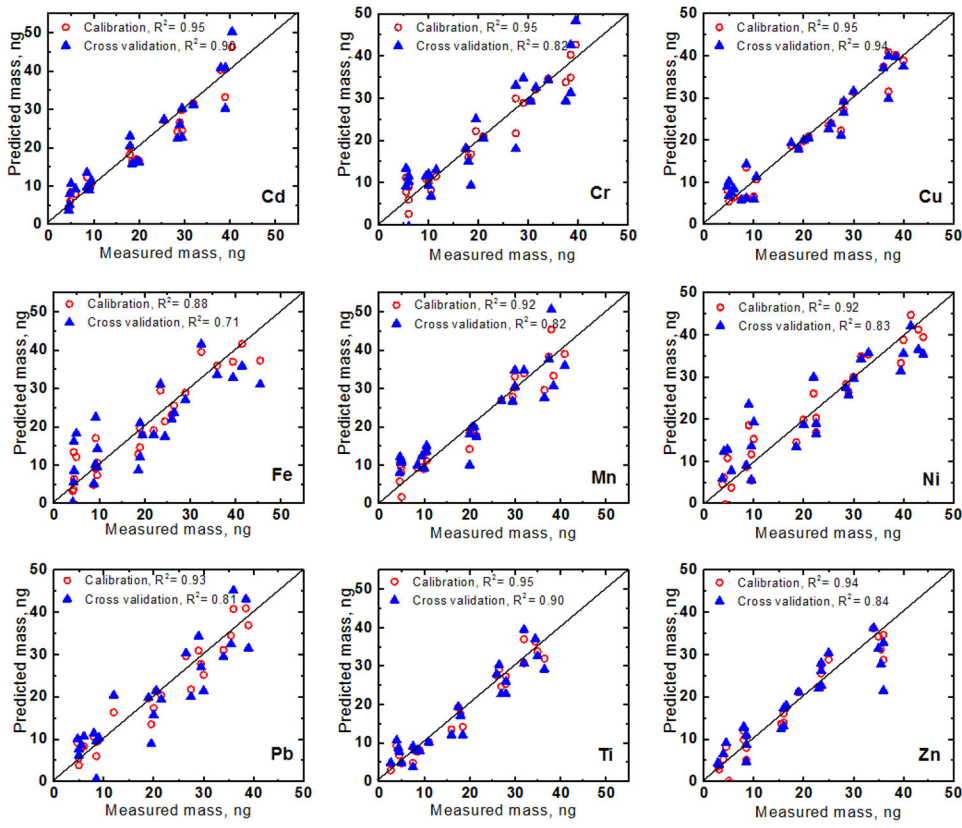


**Fig. 1.**

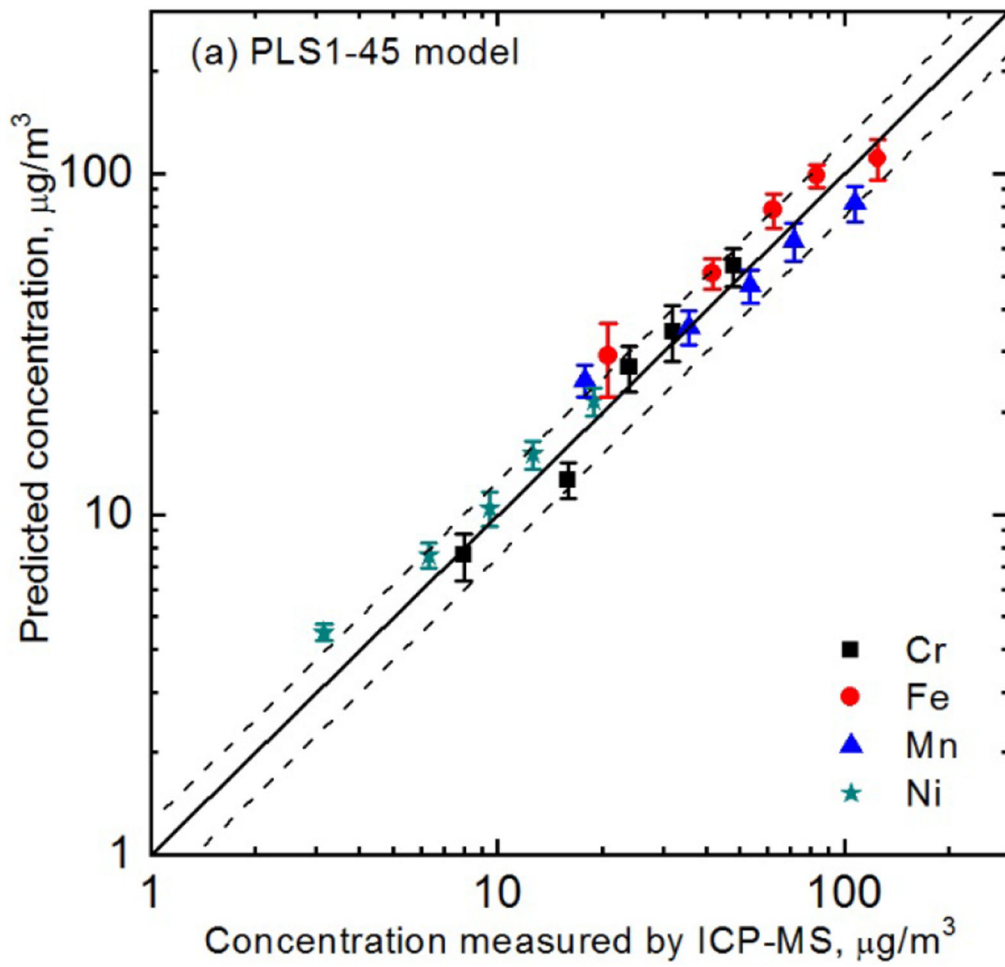
A schematic diagram of the multivariate calibration experimental procedure for measurement of aerosol elemental concentrations.

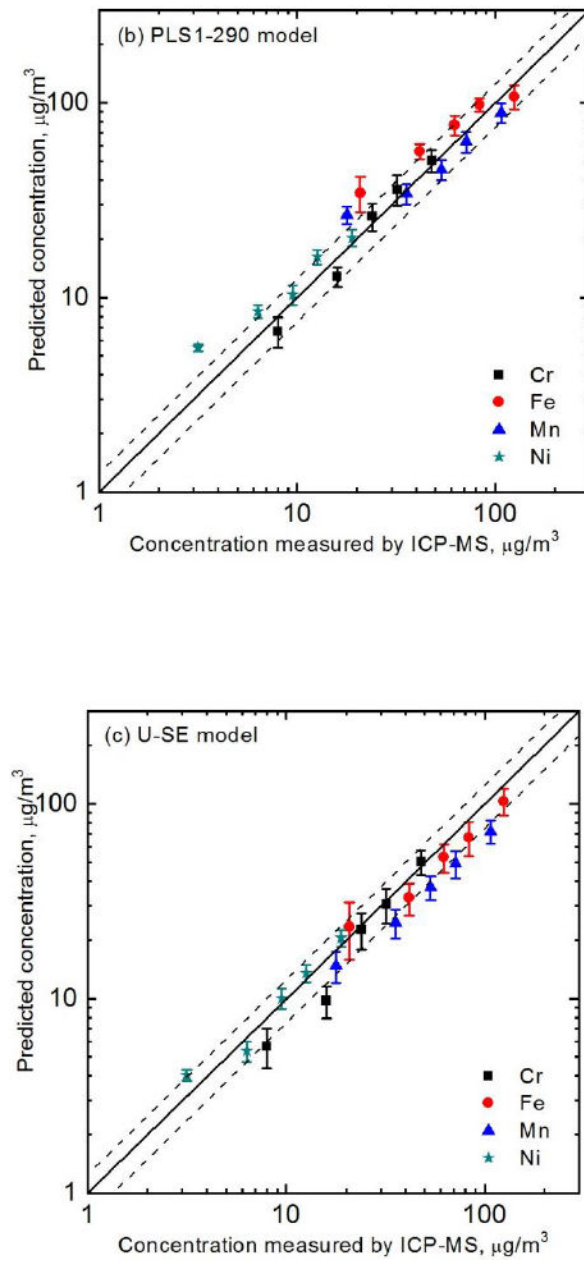


**Fig. 2.**  
PLS Regression coefficients for chromium by analysis of the full range spectra (300 – 540 nm).



**Fig. 3.**  
Predicted vs measured elemental mass in the collected particle samples for PLS1-45 models.



**Fig. 4.**

Comparison of elemental concentrations predicted by regression models (a) PLS1-45 model, (b) PLS1-290 model and (c) U-SE model, and concentrations measured by ICP-MS analysis for welding aerosol measurement. The two dashed lines represent  $\pm 25\%$  error around the 1:1 line.

**Table 1.**

Elemental composition and concentration of solutions used for generating the calibration aerosol

Sample No.	Elemental concentration in the solution, mg/L								
	Cr	Mn	Fe	Ni	Cu	Zn	Cd	Pb	Ti
1	20	20	20	20	20	20	20	20	20
2	20	5	10	5	40	40	20	10	40
3	5	10	5	40	40	20	10	40	10
4	10	5	40	40	20	10	40	10	30
5	5	40	40	20	10	40	10	30	30
6	40	40	20	10	40	10	30	30	20
7	40	20	10	40	10	30	30	20	40
8	20	10	40	10	30	30	20	40	30
9	10	40	10	30	30	20	40	30	40
10	40	10	30	30	20	40	30	40	5
11	10	30	30	20	40	30	40	5	5
12	30	30	20	40	30	40	5	5	20
13	30	20	40	30	40	5	5	20	30
14	20	40	30	40	5	5	20	30	5
15	40	30	40	5	5	20	30	5	30
16	30	40	5	5	20	30	5	30	10
17	40	5	5	20	30	5	30	10	10
18	5	5	20	30	5	30	10	10	20
19	5	20	30	5	30	10	10	20	5
20	20	30	5	30	10	10	20	5	10
21	30	5	30	10	10	20	5	10	5
22	5	30	10	10	20	5	10	5	40
23	30	10	10	20	5	10	5	40	40
24	10	10	20	5	10	5	40	40	20
25	10	20	5	10	5	40	40	20	10

**Table 2.**

Elemental mass of the aerosol samples collected by the CAM determined by ICP-MS.

Sample No.	Elemental mass, ng								
	Cr	Mn	Fe	Ni	Cu	Zn	Cd	Pb	Ti
1	21.0	21.5	19.5	22.5	25.5	19.0	20.0	20.5	17.5
2	18.5	5.0	8.8	4.3	37.0	34.0	18.0	8.5	32.0
3	6.0	9.5	4.4	40.0	36.0	15.5	8.5	35.5	8.0
4	10.5	5.0	39.5	43.0	21.0	8.5	39.0	12.0	27.0
5	6.0	41.0	45.5	22.5	10.5	36.0	9.5	30.0	28.0
6	37.5	38.5	18.6	9.5	37.0	8.5	28.5	29.5	18.0
7	38.5	20.5	9.5	41.5	10.0	23.5	29.0	20.0	34.5
8	19.5	10.5	32.5	10.0	28.0	23.5	19.5	38.5	26.5
9	10.0	38.0	9.2	30.0	28.0	16.0	38.0	29.0	32.0
10	38.5	10.5	24.5	31.5	20.0	35.0	29.5	39.0	2.6
11	11.5	30.0	29.0	22.0	38.5	25.0	39.0	6.0	5.0
12	31.5	32.0	19.0	44.0	30.0	36.0	6.0	5.5	18.5
13	30.5	21.0	36.0	33.0	40.0	5.0	5.0	19.5	26.0
14	18.0	36.5	26.5	39.5	5.0	4.5	18.5	27.5	3.9
15	39.5	30.0	41.5	5.5	5.0	16.5	29.5	5.0	28.0
16	27.5	37.5	4.3	4.0	17.5	23.5	4.7	26.5	8.5
17	34.0	4.6	4.1	18.5	25.0	3.1	25.5	9.0	7.5
18	5.5	4.7	22.0	28.5	4.7	23.0	8.5	8.0	11.0
19	5.5	20.0	23.5	4.8	27.5	8.5	9.0	19.0	4.3
20	17.5	27.0	4.4	29.0	8.5	8.0	18.0	4.8	7.5
21	27.5	4.9	26.0	8.5	8.5	16.0	4.5	8.5	4.5
22	6.0	29.5	9.2	9.0	19.0	3.9	9.0	5.0	36.5
23	29.0	10.0	9.6	20.0	6.0	8.0	4.8	36.0	35.0
24	9.5	8.5	19.0	3.7	7.5	2.8	32.0	34.0	16.0
25	10.0	20.0	4.9	9.5	5.5	35.5	40.5	21.5	9.0

**Table 3.**

Selected elemental emission lines for each element investigated in this study.

Elements	Emission lines/nm
Cr	425.43, 427.48, 428.97, 520.45, 520.60, 520.84, 529.82, <b>534.58</b>
Mn	344.20, 346.03, 347.40, 348.29, <b>403.08</b> , 403.31, 403.45, 482.35
Fe	374.56, 404.58, 406.36, 438.35, <b>526.95</b>
Ni	300.25, 341.48, 344.63, 345.29, 345.85, 346.17, 349.29, 351.03, 351.51, <b>352.45</b> , 356.64, 361.94
Cu	510.55, <b>521.82</b>
Zn	468.01, 472.22, <b>481.05</b> , 491.16, 492.40
Cd	361.05, 467.82, 479.99, 508.58, 533.75, <b>537.81</b>
Pb	<b>405.78</b> , 424.49, 438.65
Ti	334.94, 338.03, 338.38, 375.93, 453.32, 453.48, <b>498.17</b> , 499.11, 499.95

\* The emission lines highlighted in bold are chosen to construct PLS1-45 regression model and univariate regression model for each element.

**Table 4.**

Comparison of relative RMSECV and  $R^2$  from PLS1 and PLS2 models and those from U-ME models. The  $R^2$  values for U-ME are for calibration curves based on peak height; those based on peak area are shown in the parenthesis.

Element	$R^2$					
	PLS2-4312	PLS2-290	PLS2-45	PLS1-4312	PLS1-290	PLS1-45
Cr	0.73	0.73	0.81	0.78	0.79	0.82
Mn	0.66	0.71	0.76	0.73	0.78	0.82
Fe	0.20	0.62	0.7	0.26	0.68	0.71
Ni	0.58	0.74	0.75	0.66	0.84	0.83
Cu	0.69	0.88	0.90	0.80	0.90	0.94
Zn	0.60	0.83	0.80	0.68	0.79	0.84
Cd	0.87	0.88	0.90	0.90	0.90	0.90
Pb	0.15	0.47	0.76	0.20	0.64	0.81
Ti	0.67	0.81	0.88	0.82	0.82	0.89
Average	0.57	0.74	0.81	0.65	0.79	0.84

Element	Relative RMSECV, %					
	PLS2-4312	PLS2-290	PLS2-45	PLS1-4312	PLS1-290	PLS1-45
Cr	32	32	27	29	28	26
Mn	38	35	32	34	30	27
Fe	58	40	35	56	37	35
Ni	46	36	36	44	28	30
Cu	35	22	20	27	20	16
Zn	37	24	26	33	27	23
Cd	23	22	20	20	20	21
Pb	56	45	30	55	37	27
Ti	35	26	20	25	25	19
Average	40	31	27	36	28	25

**Table 5.**

Limits of detection of aerosol spark emission spectroscopy

Elements	Limits of detection			
	In terms of mass, ng		In terms of air concentration <sup>*</sup> , $\mu\text{g}/\text{m}^3$	
	Multivariate calibration (PLS1-45)	Univariate calibration (U-ME)	Multivariate calibration (PLS1-45)	Univariate calibration (U-ME)
Cr	1.5	1.8	0.28	0.36
Mn	1.2	1.8	0.24	0.36
Fe	2.5	3.9	0.50	0.78
Ni	2.0	3.5	0.40	0.70
Cu	1.1	1.3	0.22	0.26
Zn	1.8	2.1	0.36	0.42
Cd	0.8	1.3	0.16	0.26
Pb	2.4	4.0	0.48	0.80
Ti	1.1	1.1	0.22	0.22

<sup>\*</sup> Assuming a flow rate of 2 L min<sup>-1</sup> and a sample collection time of 5 min.